Ab Initio Prediction of Piezoelectricity in Two-Dimensional Materials

Michael N. Blonsky,[†] Houlong L. Zhuang,[†,§] Arunima K. Singh,[†] and Richard G. Hennig[*,†,‡]

[†]Department of Materials Science and Engineering, Cornell University, Ithaca, New York 14853, United States and [‡]Department of Materials Science and Engineering, University of Florida, Gainesville, Florida 32611, United States. [§]Present address (H.L.Z.): Department of Mechanical and Aerospace Engineering, Princeton University, Princeton, New Jersey 08544, United States.

ABSTRACT Two-dimensional (2D) materials present many unique materials concepts, including material properties that sometimes differ dramatically from those of their bulk counterparts. One of these properties, piezoelectricity, is important for micro- and nanoelectromechanical systems applications. Using symmetry analysis, we determine the independent piezoelectric coefficients for four groups of predicted and synthesized 2D materials. We calculate with density-functional perturbation theory the stiffness and piezoelectric tensors of these materials. We determine the in-plane piezoelectric coefficient d_{11} for 37 materials within the families of 2D metal dichalcogenides, metal oxides, and III–V semiconductor materials. A majority of the structures, including $CrSe_2$, $CrTe_2$, CaO, CdO, ZnO, and InN, have d_{11} coefficients greater than 5 pm/V, a typical value for bulk piezoelectric materials. Our symmetry analysis shows that buckled 2D materials exhibit an out-of-plane coefficient d_{31}. We find that d_{31} for 8 III–V semiconductors ranges from 0.02 to 0.6 pm/V. From statistical analysis, we identify correlations between the piezoelectric coefficients and the electronic and structural properties of the 2D materials that elucidate the origin of the piezoelectricity. Among the 37 2D materials, CdO, ZnO, and $CrTe_2$ stand out for their combination of large piezoelectric coefficient and low formation energy and are recommended for experimental exploration.

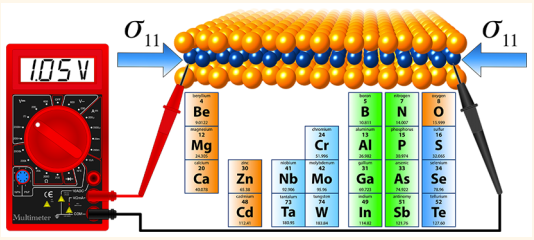

KEYWORDS: piezoelectricity · 2D materials · density-functional theory · electronic and structural properties · metal dichalcogenides · group-II oxides · group III–V compounds

Two-dimensional (2D) materials can exhibit significantly different and sometimes unique or surprising properties compared to their bulk counterparts. Examples include the high mechanical strength and electrical conductivity of graphene,[1−3] the high photocatalytic activity for water splitting of 2D SnS_2,[4,5] the predicted remarkable optical and magnetic properties of doped 2D BN,[6] and the promising electronic bandgaps and band edge positions of 2D dichalcogenide and monochalcogenide materials for semiconductor and photocatalysis applications.[7−10]

Another particularly interesting and useful property of 2D materials is piezoelectricity, which allows for energy conversion between electrical and mechanical energy. Nanoscale piezoelectric materials have a wide variety of applications as sensors, actuators, transducers, and energy harvesters in the fields of nanorobotics, piezotronics, and nanoelectromechanical systems.[11−18] Understanding and quantifying piezoelectricity in 2D materials will promote the development of these applications and will help add to the Materials Genome Initiative.[19]

The reduction in dimensionality of 2D materials results in 2D crystal structures that are significantly more anisotropic (*i.e.*, have fewer symmetry elements) than bulk materials. Particularly, inversion symmetry is often eliminated in 2D structures, which allows these materials to become piezoelectric. For example, compounds exhibiting planar and buckled hexagonal[20,21] and 2*H* structures[9,11,12] all break inversion symmetry and hence can exhibit piezoelectricity.

Recent studies have predicted piezoelectricity for doped graphene, graphene oxide, single-layer hexagonal BN, and transition metal dichalcogenides.[11−13,22] The piezoelectric coefficients computed by density-functional theory range from 0.2 to 0.3 pm/V for doped graphene,[13] to 0.24 pm/V for graphene oxide,[22] to 0.6 pm/V for single-layer BN,[11] to 2–10 pm/V for 7 single-layer dichalcogenides (CrS_2, MoX_2 and WX_2 (X = S, Se, Te).[11,12] For the dichalcogenide family, the piezoelectric coefficients increase with larger chalcogen atoms and smaller group-VI atoms.[11,12] This range of values is similar in magnitude to bulk piezoelectric materials, although still much smaller

* Address correspondence to rhennig@ufl.edu.

Received for review June 1, 2015 and accepted August 27, 2015.

Published online August 27, 2015
10.1021/acsnano.5b03394

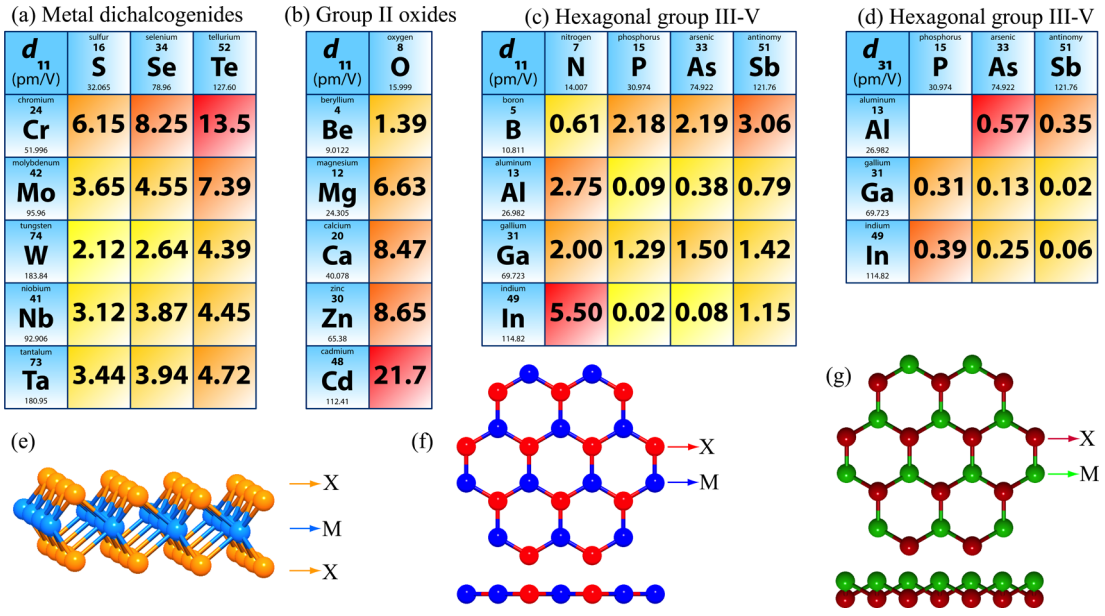

Figure 1. Periodic trends for d_{11} in (a) metal dichalcogenides, (b) metal oxides, and (c) group III−V semiconductors as well as for d_{31} in (d) group III−V semiconductors. Structures in each group with large coefficients are shaded red. Material structures are illustrated for (e) 2*H*, (f) planar hexagonal, and (g) buckled hexagonal structures.

than that of lead zirconium titanate (360 pm/V).[23] Measurements for monolayer MoS_2 show a piezoelectric coefficient of $e_{11} = 2.9 \times 10^{-10}$ C/m in good agreement with previous calculations and our study.[24]

In this letter, we specifically focus on 2D metal dichalcogenides, group IIA and IIB metal oxides, and group III−V semiconductors illustrated in Figure 1. These 2D materials exhibit sufficiently low formation energies relative to their bulk structures and therefore can be exfoliated from bulk structures or synthesized as free-standing films.[25] Some of these materials, including single-layer SnS_2,[26] MoX_2 and WX_2 (X = S, Se, Te),[27] $NbSe_2$,[28] TaS_2,[29] $TaSe_2$,[30] AlN,[31,32] BN,[33] and ZnO[34,35] have already been successfully synthesized or exfoliated. Using symmetry analysis and density-functional perturbation theory, we identify several 2D materials families that exhibit piezoelectricity and determine their piezoelectric coefficients with the goal to find suitable piezoelectric materials for nanoscale applications. Furthermore, we find that the metal dichalcogenides and oxides exhibit an in-plane piezoelectric coefficient d_{11}, while some hexagonal group III−V materials also display an additional out-of-plane coefficient d_{31}. Finally, we use statistical analysis to explore the correlation between the structures' piezoelectric coefficients and their structural, electronic, and chemical properties.

SYMMETRY ANALYSIS

The relaxed ion elastic and piezoelectric tensors are obtained as the sum of ionic and electronic contributions:

$$C_{ijkl} = \frac{d\sigma_{ij}}{d\varepsilon_{kl}} = C^{\text{ion}}_{ijkl} + C^{\text{el}}_{ijkl} \quad \text{and}$$
$$e_{ijk} = \frac{dP_i}{d\varepsilon_{jk}} = e^{\text{ion}}_{ijk} + e^{\text{el}}_{ijk} \qquad (1)$$

where σ_{ij} is the stress tensor, ε_{kl} is the strain tensor, and P_i is the intrinsic polarization tensor.

Plane-wave based DFT algorithms calculate these coefficients assuming periodic boundary conditions in a three-dimensional (3D) system. To convert these coefficients to a 2D system, we assume plane stress and plane strain conditions ($\varepsilon_{ij} = \sigma_{ij} = 0$ for $i = 3$ or $j = 3$). We do not limit the polarization to remain in-plane, as done in other derivations.[36] For all considered 2D structures, we define the in-plane directions x_1 and x_2 as the commonly referred to armchair and zigzag direction, respectively, and x_3 as perpendicular to the 2D layer.

Employing Voigt notation, the 2D elastic and piezoelectric tensors become:

$$C_{ij} = \begin{Bmatrix} C_{11} & C_{12} & C_{16} \\ C_{21} & C_{22} & C_{26} \\ C_{61} & C_{62} & C_{66} \end{Bmatrix} \quad \text{and}$$
$$e_{ij} = \begin{Bmatrix} e_{11} & e_{12} & e_{16} \\ e_{21} & e_{22} & e_{26} \\ e_{31} & e_{32} & e_{36} \end{Bmatrix} \qquad (2)$$

Due to 3D periodic boundary conditions, the 2D coefficients C^{2D}_{ij} and e^{2D}_{ij} must be renormalized by the z lattice parameter corresponding to the spacing between 2D layers, *i.e.*, $C^{2D}_{ij} = zC^{3D}_{ij}$ and $e^{2D}_{ij} = ze^{3D}_{ij}$. We also report the strain coefficients of the piezoelectric tensor, which is important for piezoelectric applications,

$$d_{ij} = \frac{dP_i}{d\sigma_j} \quad \text{with} \quad e_{ik} = d_{ij}C_{jk} \qquad (3)$$

Performing symmetry analysis on the elastic and piezoelectric tensors using the point groups of the 2D materials further reduces the number of independent tensor coefficients. Since all the 2D materials studied

here have at least a 3*m* point-group symmetry, we derive the expressions for the independent d_{ij} coefficients for this point group. The elastic and piezoelectric tensors become:

$$C_{ij} = \begin{Bmatrix} C_{11} & C_{12} & 0 \\ C_{12} & C_{11} & 0 \\ 0 & 0 & \frac{C_{11}-C_{12}}{2} \end{Bmatrix},$$

$$e_{ij} = \begin{Bmatrix} e_{11} & -e_{11} & 0 \\ 0 & 0 & -\frac{e_{11}}{2} \\ e_{31} & e_{31} & 0 \end{Bmatrix},$$

$$d_{ij} = \begin{Bmatrix} d_{11} & -d_{11} & 0 \\ 0 & 0 & -d_{11} \\ d_{31} & d_{31} & 0 \end{Bmatrix} \quad (4)$$

Solving for the piezoelectric coefficients d_{11} and d_{31} using eqs 3 and 4 yields

$$d_{11} = \frac{e_{11}}{C_{11}-C_{12}} \text{ and } d_{31} = \frac{e_{31}}{C_{11}+C_{12}} \quad (5)$$

The 2*H* and the planar 2D structures have $\bar{6}m2$ point group symmetry, which includes 3*m* as well as a mirror plane perpendicular to x_3. This mirror symmetry nullifies the e_{31} and d_{31} coefficients, and materials with these structures only exhibit one independent piezoelectric coefficient.

RESULTS

We calculate the elastic and piezoelectric tensors for 37 two-dimensional materials in the families of metal dichalcogenides (MX_2, M = Cr, Mo, W, Nb, Ta and X = S, Se, Te), group IIA and IIB metal oxides (MO, M = Be, Mg, Ca, Zn, Cd, Pb), and group III−V semiconductors (AX, A = B, Al, Ga, In and X = N, P, As, Sb). All of these materials with nonzero piezoelectric coefficients exhibit hexagonal symmetry and have either a planar hexagonal, a buckled hexagonal, or a 2*H* structure. We note that SnX_2 and VX_2 dichalcogenides have a 1*T* structure, which displays inversion symmetry and therefore no piezoelectricity.

Figure 1 summarizes the piezoelectric coefficients d_{ij} and illustrates the crystal structures for each 2D material. Tables 1−3 show the calculated elastic and piezoelectric coefficients for all 37 materials. We report all in-plane piezoelectric coefficients, d_{11} and e_{11}, in Tables 1 and 2, as well as each structure's formation energy with reference to its bulk structure.[20,39] Most structures reported are the most stable 2D structure known, but we specify if the structure is unstable or metastable (within 10 meV/atom) compared to other 2D structures. In Table 3, we report all out-of-plane piezoelectric coefficients, d_{31} and e_{31}, for buckled hexagonal structures. The 2D tetragonal structures of AlP and PbO and the 1T structure of SnS_2 confirm our symmetry analysis; these structures have inversion centers and therefore have null piezoelectric tensors.

TABLE 1. Elastic Coefficients (C_{ij}) in Units of N/m, Piezoelectric Coefficients (e_{11}) in pC/m and d_{11} in pm/V, the Formation Energies of the 2D Materials (ΔE_f) in meV/atom Relative to the Stable Bulk Structure, and Bader Charge Transfer (ΔQ) in Electrons Per Metal Atom for the 2D Metal Dichalcogenides

material	C_{11}	C_{12}	e_{11}	d_{11}	ΔE_f	ΔQ
			Metal Dichalcogenides			
1*T*-SnS_2	71.6	17.7	0	0	80[5]	1.55
2*H*-CrS_2	122.5	34.1	543	6.15	75[12]	1.00
2*H*-$CrSe_2$	98.7	29.1	575	8.25	75	0.82
2*H*-$CrTe_2$	75.0	26.3	654	13.45	85	0.56
2*H*-MoS_2	130.3	31.0	362	3.65	77[9]	1.09
2*H*-$MoSe_2$	110.1	26.0	383	4.55	80[9]	0.80
2*H*-$MoTe_2$	83.2	20.0	467	7.39	83[9]	0.50
2*H*-WS_2	146.0	31.6	243	2.12	77[9]	1.25
2*H*-WSe_2	119.7	22.5	257	2.64	80[9]	0.92
2*H*-WTe_2	89.7	16.1	323	4.39	120[9]	0.56
2*H*-NbS_2	106.5	38.9	211	3.12	93[9]	1.58
2*H*-$NbSe_2$	89.4	32.1	222	3.87	97[9]	1.39
2*H*-$NbTe_2$	63.1	21.7	184	4.45	100[9]	1.07
2*H*-TaS_2	119.9	42.4	267	3.44	87[9]	1.57
2*H*-$TaSe_2$	98.9	35.5	250	3.94	90[9]	1.38
2*H*-$TaTe_2$	70.6	26.6	207	4.72	140[9]	1.04

DISCUSSION

To identify chemical trends for the piezoelectric coefficients within each of the various 2D materials families, we perform a principal-component analysis and subsequent multivariate regressions. We test the correlation of the piezoelectric coefficients d_{11} and d_{31} to the covalent and ionic radii, atomic polarizabilities of the atoms and ions,[40] electronegativities and Bader charges of the cation and anion species, elastic constants C_{11} and C_{12} of the 2D materials, and (only for the group 5 and 6 transition-metal dichalcogenides) the cation period. The polarizabilities are calculated using DFT and the PBE exchange-correlation functional in Gaussian09[41] employing the aug-cc-pVTZ basis set for S, Se, and Cr, and the aug-cc-pVTZ-PP basis set and pseudopotential for the heavier species Te, Nb, Mo, Ta, and W.[42]

Figure 2a illustrates a surprisingly simply correlation we obtain for the piezoelectric coefficient d_{11} in the group 5 and 6 transition-metal dichalcogenides. We discover that for these 15 materials the piezoelectric coefficients d_{11} are directly proportional to the ratio of the polarizabilities of the isolated anion and cations. This means that large piezoelectric coefficients occur for dichalcogenides with large anion and small cation polarizability. It is remarkable that this correlation holds for both the group 5 and group 6 compounds. This correlation provides insight into the underlying mechanism for piezoelectricity in the dichalcogenides. We do not observe a significant correlation of d_{11} with the Bader charges or electronegativities, which indicates that the piezoelectricity is not caused by

TABLE 2. Elastic Coefficients (C_{ij}) in Units of N/m, Piezoelectric Coefficients (e_{11}) in pC/m and d_{11} in pm/V, the Formation Energies of the 2D Materials (ΔE_f) in meV/atom Relative to the Stable Bulk Structure, and Bader Charge Transfer (ΔQ) in Electrons Per Metal Atom for the Planar (p) and Buckled (b) Hexagonal, as Well as the Square Litharge (l) and Inverted Litharge (i) 2D Group-II Oxides and Group III−V Compounds

material	C_{11}	C_{12}	e_{11}	d_{11}	ΔE_f	ΔQ
			Group-II Oxides			
BeO (p)	151.3	56.5	132	1.39	90[37]	1.69[37]
MgO (p)	85.4	50.6	230	6.63	430[37]	1.62[37]
CaO (p)	60.2	41.9	155	8.47	560[37]	0.55[37]
ZnO (p)	92.6	61.9	266	8.65	190[37]	1.18[37]
CdO (p)	68.5	53.1	333	21.7	260[37]	1.18[37]
PbO[a] (p)	50.0	46.1	280	73.1	611[38]	1.15[38]
PbO (l)	34.4	30.5	0	0	85[38]	0.94[38]
			Group III−V Compounds			
BN (p)	296.6	66.5	139	0.61	90[21]	2.10[21]
BP (p)	156.7	46.4	240	2.18	520[21]	0.54[21]
BAs (p)	134.5	41.3	204	2.19	520[21]	0.34[21]
BSb (p)	104.7	37.4	206	3.06	590[21]	0.41[21]
AlN (p)	148.1	67.1	223	2.75	510[20]	2.29[20]
AlP[a] (p)	74.1	35.0	3.5	0.09	520[20]	1.98[20]
AlP (i)	59.3	19.6	0	0	310[20]	2.04
AlAs[a] (b)	52.1	18.5	12.7	0.38	500[20]	1.77[20]
AlSb[a] (b)	39.1	14.0	19.9	0.79	480[20]	1.56[20]
GaN (p)	141.7	67.9	148	2.00	420[20]	1.34[20]
GaP[b] (b)	62.0	21.3	52.6	1.29	450[20]	0.74[20]
GaAs[b] (b)	49.3	16.7	49.0	1.50	410[20]	0.57[20]
GaSb[a] (b)	36.0	12.6	33.2	1.42	390[20]	0.27[20]
InN (p)	98.4	57.7	224	5.50	450[20]	1.22[20]
InP[b] (b)	45.3	19.0	0.5	0.02	440[20]	0.72[20]
InAs[b] (b)	35.9	14.9	1.7	0.08	410[20]	0.59[20]
InSb[a] (b)	27.6	12.0	17.9	1.15	380[20]	0.36[20]

[a] Unstable structure. [b] Metastable structure (within 10 meV/atom).

TABLE 3. 2D Out-of-Plane Piezoelectric Coefficients, e_{31} and d_{31}, for the 2D Buckled Hexagonal III−V Compounds

material	e_{31} (pC/m)	d_{31} (pm/V)
AlAs[a]	40.1	0.568
AlSb[a]	18.6	0.351
GaP[b]	25.9	0.310
GaAs[b]	8.2	0.125
GaSb[a]	0.8	0.016
InP[b]	25.1	0.390
InAs[b]	12.6	0.248
InSb[a]	2.3	0.058

[a] Unstable structure. [b] Metastable structure (within 10 meV/atom).

just a displacement of the ions but due to the change in polarization of the ions resulting from the applied strain. Furthermore, we observe that the anion and cation polarization contribute oppositely, *i.e.*, a large anion and small cation polarization maximizes d_{11}. This indicates that the change in the polarization of the anions dominates the piezoelectricity and that the cation polarization counteracts the effect.

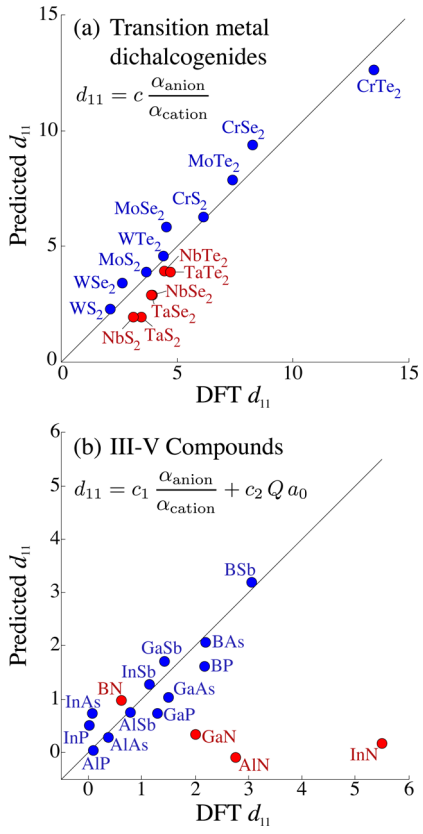

Figure 2. Correlations between the piezoelectric coefficients d_{11} of 2D materials and fundamental materials descriptors. (a) For the group 5 and 6 transition-metal dichalcogenides, we find that d_{11} is directly proportional to the ratio of the anion and cation polarizabilities. (b) For the group III−V compounds, the d_{11} is correlated to a linear combination of the ratio of the anion and cation polarizabilities and the product of the Bader charge and in-plane lattice parameter. The three nitrides, AlN, GaN, and InN, do not follow that trend.

Figure 2b shows a similar trend for the III−V 2D materials as for the transition metal dichalcogenides. In the case of the III−V 2D materials, we observe that the piezoelectric coefficient d_{11} is correlated to a linear combination of two materials descriptors, the ratio of the anion and cation polarizabilities and the product of the Bader charge and lattice parameter. This indicates that in this materials class, the piezoelectricity originates from both the change in polarization of the ions due to strain and the displacement of the ions. We note that while 13 of the III−V materials follow this trend, it does not hold for AlN, GaN, and InN, possibly due to the large electronegativity and small size of nitrogen compared to the other pnictogens. Interestingly, the observed trend for the 13 III−V materials holds across the planar and buckled 2D materials structures.

The piezoelectric coefficients of the 2D materials span a significant range, with most d_{11} in the 1−10 pm/V range. This is very similar to many important bulk piezoelectric materials, including α-quartz (2.3 pm/V), GaN (3.1 pm/V), and AlN (5.1 pm/V).[43,44] Several of the 2D metal oxides and metal dichalcogenides (CdO, PbO, and $CrTe_2$) exhibit dielectric coefficients much larger

than those for these bulk materials, although still much smaller than d_{33} in bulk PZT (360 pm/V).[23]

Most results for in-plane piezoelectric coefficients are in good agreement with previously calculations with differences for d_{11} of about 4%. These differences are likely due to small errors in elastic constants and alternative computational methods for determining e_{11}; for example, ref 11 did not employ DFPT. The larger discrepancy for $MoTe_2$ might be caused by the use of a different pseudopotential.[11,12]

In addition to the in-plane piezoelectric coefficient of the 2D hexagonal materials, we also identified a previously unreported out-of-plane piezoelectric coefficient d_{31} and e_{31} in the buckled hexagonal 2D materials. It describes the piezoelectric effect in which a stress or strain along the plane of the 2D material induces a change in polarization perpendicular to the atomic plane. We observe this effect for the buckled hexagonal structures that display a significant electric dipole in the direction perpendicular to the 2D layer. However, all of the buckled 2D structures we investigated are energetically metastable compared to reported 2D tetragonal structures with their formation energies being 10−320 meV/atom higher than those 2D tetragonal structures.[20] However, it is feasible or even likely that some of these 2D structures can be stabilized on a suitable hexagonal substrate that is symmetry and lattice matched.[45,46] The perpendicular polarization direction may allow these materials to be used in many more 2D piezoelectric applications. Furthermore, it is the only nonzero piezoelectric effect we observe when 2D materials are subject to isotropic stress conditions, $\sigma_1 = \sigma_2$. This effect presents the possibility for novel device geometries and a wider variety of nanoscale piezoelectric applications.

Given the sizable piezoelectric coefficients of many 2D materials and their reasonably low formation energies relative to their bulk counterparts, we believe that many of these materials are good candidates for nanoscale piezoelectric applications. Specifically, we highlight $CrSe_2$, $CrTe_2$, CdO, ZnO, and InN for their large d_{11} coefficients and low formation energies and InP and AlAs for their large d_{31} coefficients. Further computational studies could determine the effect of substrates on the stability and piezoelectric properties of these 2D materials.

CONCLUSIONS

We report piezoelectric coefficients for multiple 2D material systems, including group III−V semiconductors, metal dichalchogenides, and metal oxides. Notable systems with high d_{11} coefficients include $CrSe_2$ (8.25 pm/V), $CrTe_2$ (13.45 pm/V), CaO (8.47 pm/V), CdO (21.7 pm/V), ZnO (8.65 pm/V), and InN (5.50 pm/V). We also report a new piezoelectric effect in buckled 2D structures that generates a polarization perpendicular to the material layer with InP and AlAs displaying the largest d_{31} coefficients of 0.39 and 0.57 pm/V. We identify correlations for each group of 2D materials to help predict optimal material systems for nanoscale piezoelectric applications. Finally, we suggest experimental work for some systems given their high stability and applicable piezoelectric coefficients. These results provide valuable guidance for experimental synthesis efforts and potential applications of 2D materials.

METHODS

We perform density-functional theory (DFT) calculations using the projector-augmented wave method as implemented in the plane-wave code VASP.[47−49] The DFT calculations for the structural relaxation and the calculations of the elastic and piezoelectric tensors employ the Perdew−Burke−Ernzerhof exchange-correlation functional.[50] For the formation energies of the 2D transition metal dichalcogenide materials relative to their layered bulk structures, we use the nonlocal vdW-DF-optB88 exchange-correlation functional.[51−53] The van der Waals functional accurately describes the dispersion interactions in multilayered transition metal dichalcogenides[12,54] and the physisorption of 2D materials on substrates.[55] For the structural relaxations, a cutoff energy of 450 eV for the plane wave basis set and a $30 \times 30 \times 1$ k-point mesh ensure an accuracy of the energy of 2 meV/atom. We find that a vacuum spacing of 15 Å is sufficient to reduce the interactions between the layers to below 1 meV/atom. We calculate the elastic tensor coefficients, C_{ijkl}, including ionic relaxations using the finite differences method[56] and the strain coefficients of the piezoelectric tensor, e_{ijk}, using density-functional perturbation theory (DFPT).[56]

The piezoelectric coefficients are converged with respect to the vacuum spacing by systematically increasing the spacing between the layers up to 30 Å. We observe that a spacing of 15 Å is sufficient to converge the piezoelectric coefficient e_{11} for the planar hexagonal and the 2H structures. The buckled hexagonal materials, however, require a larger spacing to converge the piezoelectric coefficients to within 1% accuracy due to larger electrostatic interactions. Instead of further increasing the layer spacing, which becomes computationally demanding, we extrapolate the in-plane piezoelectric coefficient, e_{11}, to infinite spacing by fitting the values to the inverse of the layer spacing. For the out-of-plane coefficient, e_{31}, we find that a fit of the values to the square inverse of the layer spacing allows for an efficient extrapolation.

Conflict of Interest: The authors declare no competing financial interest.

Acknowledgment. This work was supported by the NSF under the CAREER Award No. DMR-1056587 and under Award No. ACI-1440547. This research used computational resources of the Texas Advanced Computing Center under Contract No. TG-DMR050028N and the Extreme Science and Engineering Discovery Environment (XSEDE), which is supported by National Science Foundation grant number ACI-1053575.

REFERENCES AND NOTES

1. Lee, C.; Wei, X.; Kysar, J. W.; Hone, J. Measurement of the Elastic Properties and Intrinsic Strength of Monolayer Graphene. *Science* **2008**, *321*, 385–388.
2. Ruiz-Vargas, C. S.; Zhuang, H. L.; Huang, P. Y.; van der Zande, A. M.; Garg, S.; McEuen, P. L.; Muller, D. A.; Hennig,

R. G.; Park, J. Softened Elastic Response and Unzipping in Chemical Vapor Deposition Graphene Membranes. *Nano Lett.* **2011**, *11*, 2259–2263.
3. Novoselov, K. S.; Geim, A. K.; Morozov, S. V.; Jiang, D.; Zhang, Y.; Dubonos, S. V.; Grigorieva, I. V.; Firsov, A. A. Electric Field Effect in Atomically Thin Carbon Films. *Science* **2004**, *306*, 666–669.
4. Sun, Y.; Cheng, H.; Gao, S.; Sun, Z.; Liu, Q.; Liu, Q.; Lei, F.; Yao, T.; He, J.; Wei, S.; et al. Freestanding Tin Disulfide Single-Layers Realizing Efficient Visible-Light Water Splitting. *Angew. Chem., Int. Ed.* **2012**, *51*, 8727–8731.
5. Zhuang, H. L.; Hennig, R. G. Theoretical Perspective of Photocatalytic Properties of Single-Layer SnS_2. *Phys. Rev. B: Condens. Matter Mater. Phys.* **2013**, *88*, 115314.
6. Park, H.; Wadehra, A.; Wilkins, J. W.; Castro Neto, A. H. Magnetic States and Optical Properties of Single-Layer Carbon-Doped Hexagonal Boron Nitride. *Appl. Phys. Lett.* **2012**, *100*, 253115.
7. Lebègue, S.; Björkman, T.; Klintenberg, M.; Nieminen, R. M.; Eriksson, O. Two-Dimensional Materials from Data Filtering and Ab Initio Calculations. *Phys. Rev. X* **2013**, *3*, 031002.
8. Tongay, S.; Zhou, J.; Ataca, C.; Lo, K.; Matthews, T. S.; Li, J.; Grossman, J. C.; Wu, J. Thermally Driven Crossover from Indirect toward Direct Bandgap in 2D Semiconductors: $MoSe_2$ versus MoS_2. *Nano Lett.* **2012**, *12*, 5576–5580.
9. Zhuang, H. L.; Hennig, R. G. Computational Search for Single-Layer Transition-Metal Dichalcogenide Photocatalysts. *J. Phys. Chem. C* **2013**, *117*, 20440–20445.
10. Zhuang, H. L.; Hennig, R. G. Single-Layer Group-III Monochalcogenide Photocatalysts for Water Splitting. *Chem. Mater.* **2013**, *25*, 3232–3238.
11. Duerloo, K.-A. N.; Ong, M. T.; Reed, E. J. Intrinsic Piezoelectricity in Two-Dimensional Materials. *J. Phys. Chem. Lett.* **2012**, *3*, 2871–2876.
12. Zhuang, H. L.; Johannes, M. D.; Blonsky, M. N.; Hennig, R. G. Computational Prediction and Characterization of Single-Layer CrS_2. *Appl. Phys. Lett.* **2014**, *104*, 022116.
13. Ong, M. T.; Reed, E. J. Engineered Piezoelectricity in Graphene. *ACS Nano* **2012**, *6*, 1387–1394.
14. Kaul, A. B.; Wong, E. W.; Epp, L.; Hunt, B. D. Electromechanical Carbon Nanotube Switches for High-Frequency Applications. *Nano Lett.* **2006**, *6*, 942–947.
15. Zhang, C.; Chen, W.; Zhang, C. Two-Dimensional Theory of Piezoelectric Plates Considering Surface Effect. *Eur. J. Mech. A-Solids* **2013**, *41*, 50–57.
16. Kim, K.-H.; Kumar, B.; Lee, K. Y.; Park, H.-K.; Lee, J.-H.; Lee, H. H.; Jun, H.; Lee, D.; Kim, S.-W. Piezoelectric Two-Dimensional Nanosheets/Anionic Layer Heterojunction for Efficient Direct Current Power Generation. *Sci. Rep.* **2013**, *3*, 2017.
17. Lanza, M.; Reguant, M.; Zou, G.; Lv, P.; Li, H.; Chin, R.; Liang, H.; Yu, D.; Zhang, Y.; Liu, Z.; et al. High-Performance Piezoelectric Nanogenerators Using Two-Dimensional Flexible Top Electrodes. *Adv. Mater. Interfaces* **2014**, *1*, 1300101.
18. Wu, W.; Wang, L.; Li, Y.; Zhang, F.; Lin, L.; Niu, S.; Chenet, D.; Zhang, X.; Hao, Y.; Heinz, T. F.; et al. Piezoelectricity of Single-Atomic-Layer MoS_2 for Energy Conversion and Piezotronics. *Nature* **2014**, *514*, 470–474.
19. Materials Genome Initiative. 2015; https://www.whitehouse.gov/mgi.
20. Zhuang, H. L.; Singh, A. K.; Hennig, R. G. Computational Discovery of Single-Layer III-V Materials. *Phys. Rev. B: Condens. Matter Mater. Phys.* **2013**, *87*, 165415.
21. Zhuang, H. L.; Hennig, R. G. Electronic Structures of Single-Layer Boron Pnictides. *Appl. Phys. Lett.* **2012**, *101*, 153109.
22. Chang, Z.; Yan, W.; Shang, J.; Liu, J. Z. Piezoelectric Properties of Graphene Oxide: A first-principles computational study. *Appl. Phys. Lett.* **2014**, *105*, 023103.
23. Low, T. S.; Guo, W. Modeling of a Three-Layer Piezoelectric Bimorph Beam with Hysteresis. *J. Microelectromech. Syst.* **1995**, *4*, 230–237.
24. Zhu, H.; Wang, Y.; Xiao, J.; Liu, M.; Xiong, S.; Wong, Z. J.; Ye, Z.; Ye, Y.; Yin, X.; Zhang, X. Observation of Piezoelectricity in Free-Standing Monolayer MoS_2. *Nat. Nanotechnol.* **2015**, *10*, 151–155.
25. Singh, A. K.; Mathew, K.; Zhuang, H. L.; Hennig, R. G. Computational Screening of 2D Materials for Photocatalysis. *J. Phys. Chem. Lett.* **2015**, *6*, 1087–1098.
26. Song, H. S.; Li, S. L.; Gao, L.; Xu, Y.; Ueno, K.; Tang, J.; Cheng, Y. B.; Tsukagoshi, K. High-Performance Top-Gated Monolayer SnS_2 Field-Effect Transistors and their Integrated Logic Circuits. *Nanoscale* **2013**, *5*, 9666–9670.
27. Wang, Q. H.; Kourosh, K.-Z.; Andras, A.; Coleman, J. N.; Strano, M. S. Electronics and Optoelectronics of Two-Dimensional Transition Metal Dichalcogenides. *Nat. Nanotechnol.* **2012**, *7*, 699–712.
28. Castellanos-Gomez, A.; Agraït, N.; Rubio-Bollinger, G. Optical Identification of Atomically Thin Dichalcogenide Crystals. *Appl. Phys. Lett.* **2010**, *96*, 213116.
29. Zeng, Z.; Tan, C.; Huang, X.; Bao, S.; Zhang, H. Growth of Noble Metal Nanoparticles on Single-Layer TiS_2 and TaS_2 Nanosheets For Hydrogen Evolution Reaction. *Energy Environ. Sci.* **2014**, *7*, 797–803.
30. Renteria, J.; Samnakay, R.; Jiang, C.; Pope, T. R.; Goli, P.; Yan, Z.; Wickramaratne, D.; Salguero, T. T.; Khitun, A. G.; Lake, R. K.; et al. All-Metallic Electrically Gated 2H-$TaSe_2$ Thin-Film Switches and Logic Circuits. *J. Appl. Phys.* **2014**, *115*, 034305.
31. Tsipas, P.; Kassavetis, S.; Tsoutsou, D.; Xenogiannopoulou, E.; Golias, E.; Giamini, S. A.; Grazianetti, C.; Chiappe, D.; Molle, A.; Fanciulli, M.; et al. Evidence for Graphite-Like Hexagonal AlN Nanosheets Epitaxially Grown on Single Crystal Ag(111). *Appl. Phys. Lett.* **2013**, *103*, 251605.
32. Malin, T.; Mansurov, V.; Galitsyn, Y.; Zhuravlev, K. 2D AlN Crystal Phase Formation on (0001) Al_2O_3 Surface by Ammonia MBE. *Phys. Status Solidi C* **2015**, *12*, 443–446.
33. Kim, G.; Jang, A.-R.; Jeong, H. Y.; Lee, Z.; Kang, D. J.; Shin, H. S. Growth of High-Crystalline, Single-Layer Hexagonal Boron Nitride on Recyclable Platinum Foil. *Nano Lett.* **2013**, *13*, 1834–1839.
34. Deng, X.; Yao, K.; Sun, K.; Li, W.-X.; Lee, J.; Matranga, C. Growth of Single- and Bilayer ZnO on Au(111) and Interaction with Copper. *J. Phys. Chem. C* **2013**, *117*, 11211–11218.
35. Tusche, C.; Meyerheim, H. L.; Kirschner, J. Observation of Depolarized ZnO(0001) Monolayers: Formation of Unreconstructed Planar Sheets. *Phys. Rev. Lett.* **2007**, *99*, 026102.
36. Chen, S.; Li, Q.; Liu, Y.; Xue, Z. A Meshless Local Natural Neighbour Interpolation Method for Analysis of Two-Dimensional Piezoelectric Structures. *Eng. Anal. Bound. Elem.* **2013**, *37*, 273–279.
37. Zhuang, H. L.; Hennig, R. G. Computational Identification of single-layer CdO for Electronic and Optical Applications. *Appl. Phys. Lett.* **2013**, *103*, 212102.
38. Singh, A. K.; Hennig, R. G. Computational Prediction of Two-Dimensional Group-IV Mono-Chalcogenides. *Appl. Phys. Lett.* **2014**, *105*, 042103.
39. Zhuang, H. L.; Hennig, R. G. Computational Discovery, Characterization, and Design of Single-Layer Materials. *JOM* **2014**, *66*, 366–374.
40. Schwerdtfeger, P. In *Computational Aspects of Electric Polarizability Calculations: Atoms, Molecules and Clusters*; Maroulis, G., Ed.; Imperial College Press: London, 2006; pp 1−32, Updated static dipole polarizabilities are available as pdf file from the CTCP website at Massey University: http://ctcp.massey.ac.nz/dipole-polarizabilities.
41. Frisch, M. J.; Trucks, G. W.; Schlegel, H. B.; Scuseria, G. E.; Robb, M. A.; Cheeseman, J. R.; Scalmani, G.; Barone, V.; Mennucci, B.; Petersson, G. A. et al. *Gaussian 09*, Revision A.1; Gaussian, Inc.: Wallingford, CT, 2009.
42. Schuchardt, K. L.; Didier, B. T.; Elsethagen, T.; Sun, L.; Gurumoorthi, V.; Chase, J.; Li, J.; Windus, T. L. Basis Set Exchange: A Community Database for Computational Sciences. *J. Chem. Inf. Model.* **2007**, *47*, 1045–1052.
43. Bechmann, R. Elastic and Piezoelectric Constants of Alpha-Quartz. *Phys. Rev.* **1958**, *110*, 1060–1061.
44. Lueng, C. M.; Chan, H. L. W.; Surya, C.; Choy, C. L. Piezoelectric Coefficient of Aluminum Nitride and Gallium Nitride. *J. Appl. Phys.* **2000**, *88*, 5360–5363.

45. Singh, A. K.; Zhuang, H. L.; Hennig, R. G. *Ab initio* Synthesis of Single-Layer III-V Materials. *Phys. Rev. B: Condens. Matter Mater. Phys.* **2014**, *89*, 245431.
46. Singh, A. K.; Hennig, R. G. Computational Synthesis of Single-Layer GaN on Refractory Materials. *Appl. Phys. Lett.* **2014**, *105*, 051604.
47. Kresse, G.; Furthmüller, J. Efficient Iterative Schemes for *Ab Initio* Total-Energy Calculations Using a Plane-Wave Basis Set. *Phys. Rev. B: Condens. Matter Mater. Phys.* **1996**, *54*, 11169–11186.
48. Blöchl, P. E. Projector Augmented-Wave Method. *Phys. Rev. B: Condens. Matter Mater. Phys.* **1994**, *50*, 17953–17979.
49. Kresse, G.; Joubert, D. From Ultrasoft Pseudopotentials to the Projector Augmented-Wave Method. *Phys. Rev. B: Condens. Matter Mater. Phys.* **1999**, *59*, 1758–1775.
50. Perdew, J. P.; Burke, K.; Ernzerhof, M. Generalized Gradient Approximation Made Simple. *Phys. Rev. Lett.* **1996**, *77*, 3865–3868.
51. Klimeš, J. c. v; Bowler, D. R.; Michaelides, A. Van der Waals Density Functionals Applied to Solids. *Phys. Rev. B: Condens. Matter Mater. Phys.* **2011**, *83*, 195131.
52. Dion, M.; Rydberg, H.; Rydberg, H.; Schröder, E.; Langreth, D. C.; Lundqvist, B. I. Van der Waals Density Functional for General Geometries. *Phys. Rev. Lett.* **2004**, *92*, 246401.
53. Román-Pérez, G.; Soler, J. M. Efficient Implementation of a van der Waals Density Functional: Application to Double-Wall Carbon Nanotubes. *Phys. Rev. Lett.* **2009**, *103*, 096102.
54. Björkman, T.; Gulans, A.; Krasheninnikov, A. V.; Nieminen, R. M. Van der Waals Bonding in Layered Compounds from Advanced Density-Functional First-Principles Calculations. *Phys. Rev. Lett.* **2012**, *108*, 235502.
55. Hwang, J.; Kim, M.; Campbell, D.; Alsalman, H. A.; Kwak, J. Y.; Shivaraman, S.; Woll, A. R.; Singh, A. K.; Hennig, R. G.; Gorantla, S.; et al. Van der Waals Epitaxial Growth of Graphene on Sapphire by Chemical Vapor Deposition without a Metal Catalyst. *ACS Nano* **2013**, *7*, 385–395.
56. Wu, X.; Vanderbilt, D.; Hamann, D. R. Systematic Treatment Of Displacements, Strains, and Electric Fields in Density-Functional Perturbation Theory. *Phys. Rev. B: Condens. Matter Mater. Phys.* **2005**, *72*, 035105.